Theoretical Chemistry Accounts (2020) 139:119
https://doi.org/10.1007/s00214-020-02627-7

REGULAR ARTICLE

A DFT study on the molecular mechanism of the conjugated nitroalkenes polymerization process initiated by selected unsaturated nucleophiles

Agnieszka Kącka-Zych[1] · **Radomir Jasiński**[1]

Received: 14 April 2020 / Accepted: 8 June 2020 / Published online: 19 June 2020

Abstract
The participation of the nitroethene and its α-substituted analogs as model nitrofunctionalized monomers, and (Z)-C,N-diphenylnitrone and methyl vinyl ether as initiators in the polymerization reactions, has been analyzed in the framework of the density functional theory calculations at the M06-2X(PCM)/6-311 + G(d) level. Our computational study suggests the zwitterionic mechanism of the polymerization process. The exploration of the nature of critical structures shows that the first reaction stage exhibits evidently polar nature, whereas additions of further nitroalkene molecules to the polynitroalkyl molecular system formed should be considered as moderate polar processes. The more detailed view on the molecular transformations gives analysis based on the bonding evolution theory. This study shows that the case of polymerization reaction between nitroethene and (Z)-C,N-diphenylnitrone allows for distinguishing eleven topologically different phases, while, in the case of polymerization reaction nitroethene and methyl vinyl ether, we can distinguish nine different phases.

Keywords Nitroalkenes · Polymerization process · Bonding evolution theory · Electron localization function · Molecular electron density theory

1 Introduction

Poly-nitro compounds are widely used as highly effective propellants [1]. The general method for their preparation is the polymerization of conjugated nitroalkenes (CNA) [2]. However, not all nitroalkenes can be used as raw material in this kind of synthesis. In particular, it is much easier for a retro-nitroaldol reaction to take place with 2-aryl-1-EWG-1-nitroethenes, and addition reactions only apply to some highly reactive nucleophilic reagents such as azide ion [3], cyclopentadiene [4] and N-methylazomethine ylide [5]. 2-Aryl-1-nitroethenes of the retro-nitroaldol reaction are not participated and, at the same time, are effective components of addition to dienes [6, 7] and three-atom components (TACs) [8] such as nitrones [9, 10], azides [11] and nitrile N-oxides [12–14]. At the same time, there are no reports about their polymerization. On the other hand, parent nitroethene (**1a**) [15] and its simple 1-substituted analogs such as 2-nitroprop-1-ene (**1b**) [15, 16], 1-fluoro-1-nitroethene (**1c**) [17], 1-chloro-1-nitroethene (**1d**) [18, 19] or 1-bromo-1-nitroethene (**1e**) [20] tend to form high molecular systems (Scheme 1). The initiators described for this type of polymerization are inorganic bases [15, 16]. The disadvantage of their use is the quite rapid and sometimes explosive polymerization process. The milder CNA polymerization processes have not been the subject of detailed research work so far.

Huisgen and Mloston described the reaction of nitroethene with 2,2,4,4-tetramethyl-3-thioxocyclobutanone S-methylide in 1992 [21]. In this reaction, the cycloadduct expected by the authors [3 + 2] is formed with relatively low yield. Instead, significant amounts of nitroethene polymer were found in the post-reaction mass. This prompted the authors to hypothesize that the first stage of the analyzed reaction is the formation of a zwitterionic adduct (**ZA**), which, as a labile intermediate, may on competitive paths (a) cyclize to nitrothiolate and (b) become the initiator of mild nitroethene polymerization (Scheme 2). Recent studies

Dedicated to Professor Grzegorz Mlostoń on the occasion of his 70th birthday.

✉ Radomir Jasiński
radomir@chemia.pk.edu.pl

[1] Department of Organic Chemistry, Cracow University of Technology, Warszawska 24, 31-155 Cracow, Poland

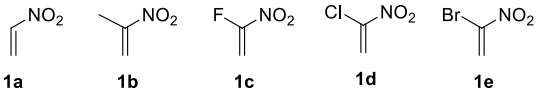

Scheme 1 Polymerizable nitroethenes

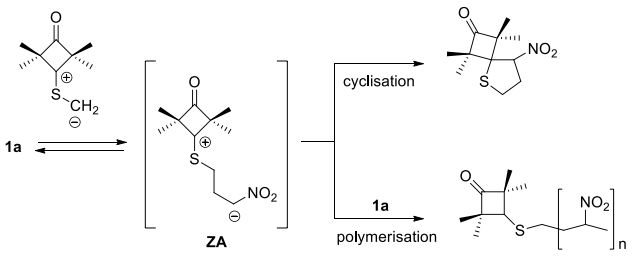

Scheme 2 Competition between [3 + 2] cycloaddition and polymerization in the reaction of nitroethene (**1a**) with 2,2,4,4-tetramethyl-3-thioxocyclobutanone S-methylide

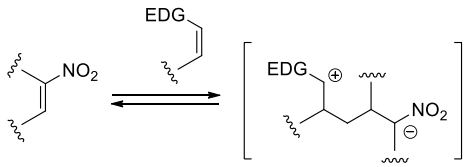

Scheme 3 The process of the formation of zwitterionic intermediates in reactions between conjugated nitroalkenes and EDG-substituted unsaturated compounds

have confirmed the presence of the zwitterionic intermediate in the environment of the described reaction [22].

In recent years, it has been observed that certain amounts of nitropolymers also appear in post-reaction masses [3 + 2] cycloaddition of nitroethene and its 1-substituted analogs (**1a–e**) with arylonitrones, in twofold to fourfold molar excess of nitroalkene [23–25].

Analysis of the literature data [26–28] also showed that, in the case of the Hetero Diels–Alder reaction with the participation of nitroalkenes and EDG-substituted unsaturated compounds (such as alkyl vinyl ethers), the formation of a zwitterionic intermediate may compete with the addition process (Scheme 3). These intermediates, by analogy with the scenario described above, could be initiators for CNA polymerization processes.

The above observations give reason to believe that some unsaturated nucleophilic reagents may be effective initiators of mild, zwitterionic polymerization of simple CNAs. As part of this work, we decided to shed light on the molecular mechanism as well as the kinetic and thermodynamic aspects of such transformations. For this purpose, we decided to use data for quantum chemical calculations based on density functional theory (DFT). The obtained results should aid understanding of the nature of transformations taking place in the course of the analyzed processes and thus allow for their rational design on a laboratory scale.

2 Computational details

All quantum chemical calculations were performed using 'Prometheus' cluster (CYFRONET regional computational center). The M06-2X functional [29] included in the GAUSSIAN 09 package [30] and the 6-311 + G(d) basis set including both diffuse and polarization functions for all relevant atoms was used. All localized stationary points have been characterized using vibrational analysis. It was found that starting molecules, intermediates and products had positive Hessian matrices. For the contrast, all transition states (**TS**) showed only one negative eigenvalue in their Hessian matrices. For all optimized transition states, intrinsic reaction coordinate (IRC) calculations have been performed. The presence of the solvent (nitromethane) in the reaction environment has been included using IEFPCM algorithm [31].

The topological analyses of the electron localization function (ELF) [32–34] were performed with the TopMod [35] program using the corresponding M06-2X(PCM)/6-311 + G(d) monodeterminantal wavefunctions. ELF calculations were computed over a grid spacing of 0.1 a.u. for each structure, and ELF localization domains were obtained for an ELF value of 0.75. For the bonding evolution theory (BET) [36] studies, the topological analysis of the ELF along the IRC was performed for a total of 136 nuclear configurations for reaction from substrates **1a**, **2** to product **Z1A** and with second molecule of **1a** to product **Z2A**. For the reaction **1a** with **3** to product **Z1B** and reaction with second molecule of **1a** leading to **Z2B**, the topological analysis of the ELF along the IRC was performed for a total of 122 nuclear configuration. BET applies Thom's catastrophe theory (CT) concepts [37–39] to the topological analysis of the gradient field of the ELF [34].

The electron localization function (ELF) [34] is a relative measure of the same spin pair density local distribution, i.e., the Pauli repulsion, in the context of monodeterminantal wavefunctions. High values of the ELF are associated with high-probability regions for electron pairing in the spirit of Lewis structures. The analysis of the gradient field or topology of ELF [32, 33] renders a partition of the molecular space into non-overlapping volumes or basins that could be associated with entities and concepts of chemical significance as atomic cores and valence regions (e.g., bonds or lone pairs). Valence basins are in turn classified depending of the number of core basins with which they share a boundary (i.e., the so-called synaptic order) [32, 33]. A complete population analysis can be performed based on

the integration of the one- and two-electron density probabilities in the ELF basins.

3 Results and discussion

We adopted nitroethene (**1a**) and a group of its substituted analogs as model CNA, as illustrated in Scheme 1. As initiators of the polymerization process, we tested (Z)-C,N-diphenylnitrone (**2**) and methyl vinyl ether (**3**) (Scheme 4). Within the scope of theoretical studies, we examined the pathways leading to the formation of primary zwitterionic intermediates as a result of the addition of CNA to the nucleophile and then examined the energy profiles of processes involving the addition of four subsequent CNA molecules. In order to better understand the molecular mechanism of these reactions, a BET study for the key stages of the polymerization reactions nitroethene (**1a**) with (Z)-C,N-diphenylnitrone (**2**) and methyl vinyl ether (**3**) was employed.

3.1 Energetical profiles and key structures for reaction involving (Z)-C,N-diphenylnitrone

The general scheme of the reaction of (Z)-C,N-diphenylnitrone **2** with nitroethene **1a** is illustrated in Scheme 5. The

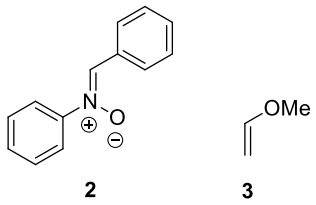

Scheme 4 Examples of potential nucleophilic initiators for zwitterionic polymerization of CNA

M06-2X(PCM)/6-311 + G(d) calculations indicate that the first stage of the process is the formation of the molecular pre-reaction complex (**MC1A**) (Fig. 1, Table 1). This is due to a decrease in the enthalpy of the reacting system by 2 kcal/mol. It should be noted that this formation causes a strong reduction in entropy, so the free Gibbs energy of **MC1A** creation is positive. This excludes the possibility of the **MC1A** complex in the form of a stable intermediate. Within **MC1A**, both of its components approach each other in such a way that the distance between the reaction centers O1 and C4 decreases below 3.5 Å. It is not a CT complex (GEDT value is equal to 0.00e). Further conversion of the pre-reaction complex is effected through transient **TS1A**. Enthalpy of **TS1A** is 7.5 kcal/mol higher than that of individual reagents. At the same time, the entropic factor causes the Gibbs free energy of the activation to be slightly higher, reaching 20 kcal/mol. Within **TS1A**, the distance between the reaction centers O1 and C4 decreases to 1.838 Å. This structure is clearly polar, as demonstrated by the value of the GEDT index (0.57 e). Further approximation of the O1 and C4 reaction centers leads to the formation of the **Z1A** intermediate. Within **Z1A**, the distance O1–C4 is 1.504 Å. This intermediate is zwitterion, which confirms the value of GEDT (0.81 e). It is not a thermodynamically stable structure and can easily undergo chemical conversion by addition of a second nitroethene molecule. This process is initiated by the formation of the **MC2A** molecular complex. This stage is carried out without overcoming the activation barrier and is associated with a decrease in enthalpy of the reacting system by 4.4 kcal/mol. The nature of **MC2A** is very similar to that of the **MC1A** complex. The gradual approach of reaction centers in this complex leads to transient **TS2A**. This involves overcoming a much lower energy barrier than in the case of the first stage of the analyzed process. Within **TS2A**, the key distance C5–C6

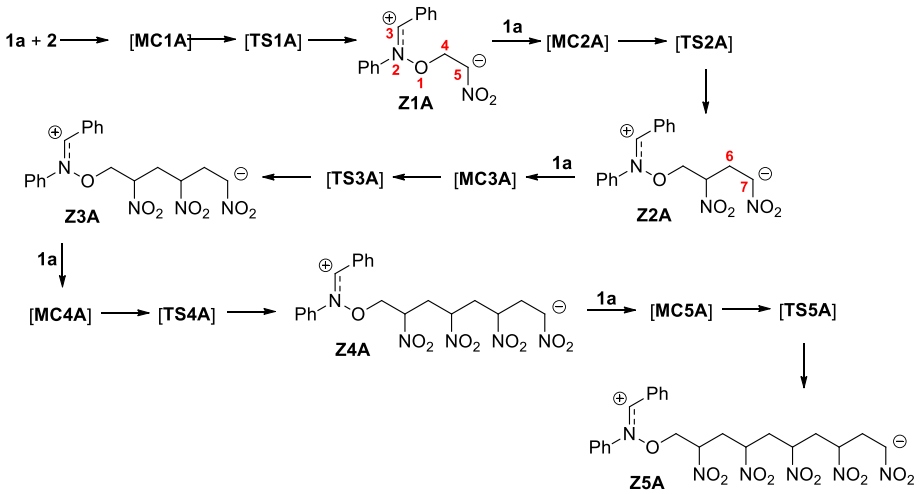

Scheme 5 Molecular mechanism of the reaction between nitroethene **1a** and (Z)-C,N-diphenylnitrone **2** according to M06-2X(PCM)/6-311 + G(d) calculations

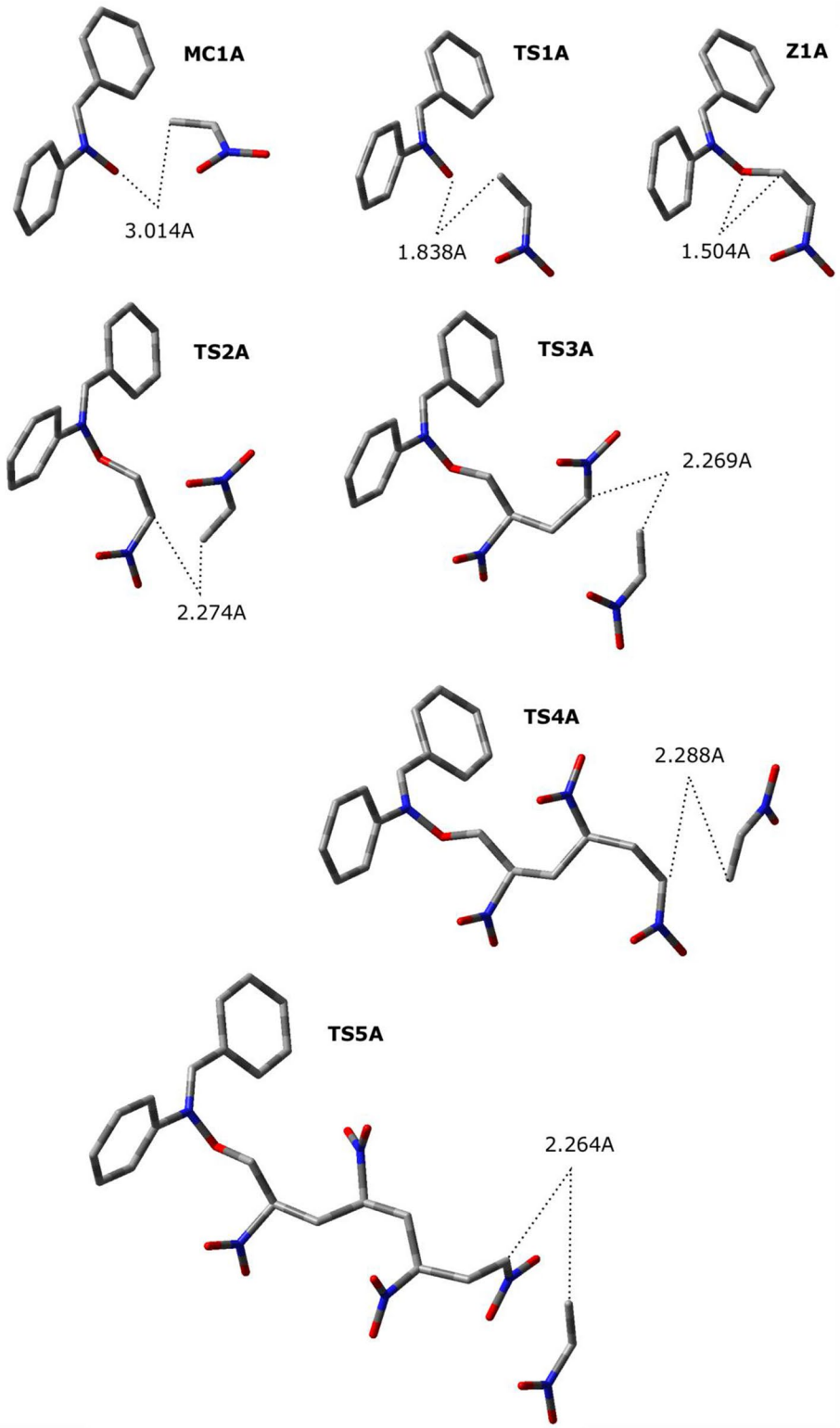

Fig. 1 Views of selected, key structures for the reaction between nitroethene **1a** and (Z)-C,N-diphenylnitrone **2** in the nitromethane solution according to M06-2X(PCM)/6-311 + G(d) calculations

reaches 2.274 Å. The polarity of **TS2A** is smaller than **TS1A** (GEDT = 0.19 e). Further movement of the reacting system along the coordinate of the reaction leads to the formation of the **Z2A** molecule. It should be emphasized that the transformation of **MC1A** into Z2A is irreversible from thermodynamic point of view. **Z2A** can add further nitroethene molecules through transient states of a nature (distances between reaction centers equal 2.26–2.29 Å; GEDT is less than 0.2 e) very similar to that of **TS2A**. The sequence of several such transformations is illustrated in

Table 1 Kinetic and thermodynamic parameters for the reaction between nitroethene **1a** and (Z)-C,N-diphenylnitrone **2** in the nitromethane solution according to M06-2X(PCM)/6-311 + G(d) calculations

Nitroalkene	Transition	ΔH (kcal/mol)	ΔS (cal/molK)	ΔG (kcal/mol)
1a	**1a + 2→MC1A**	− 2.0	− 28.2	6.4
	1a + 2→TS1A	7.5	− 41.1	19.8
	1a + 2→Z1A	5.0	− 42.3	17.6
	1a + Z1A → MC2A	− 4.4	− 34.4	5.8
	1a + Z1A → TS2A	− 0.3	− 40.4	11.8
	1a + Z1A → Z2A	− 23.3	− 43.7	− 10.3
	1a + Z2A → MC3A	− 3.6	− 33.6	6.4
	1a + Z2A → TS3A	− 1.0	− 40.2	11.0
	1a + Z2A → Z3A	− 23.6	− 46.9	− 9.6
	1a + Z3A → MC4A	− 2.7	− 25.2	4.8
	1a + Z3A → TS4A	− 0.7	− 34.8	9.7
	1a + Z3A → Z4A	− 23.3	− 37.8	− 12.0
	1a + Z4A → MC5A	− 6.3	− 42.3	6.3
	1a + Z4A → TS5A	− 3.4	− 44.7	9.9
	1a + Z4A → Z5A	− 25.0	− 45.4	− 11.5
1b	**1b + 2→MC1A**	− 6.0	− 36.9	5.0
	1b + 2→TS1A	9.5	− 43.2	22.3
	1b + 2→Z1A	7.8	− 43.2	20.6
	1b + Z1A → MC2A	− 4.9	− 36.1	5.9
	1b + Z1A → TS2A	− 1.2	− 43.8	11.9
	1b + Z1A → Z2A	− 22.5	− 49.0	− 7.9
1c	**1c + 2→MC1A**	− 1.0	− 28.6	6.7
	1c + 2→TS1A	8.3	− 40.9	20.5
	1c + 2→Z1A	5.5	− 41.0	17.7
	1c + Z1A → MC2A	− 5.1	− 37.8	6.1
	1c + Z1A → TS2A	− 1.1	− 40.3	10.9
	1c + Z1A → Z2A	− 29.7	− 45.0	− 16.3
1d	**1d + 2→MC1A**	− 8.2	− 38.8	3.3
	1d + 2→TS1A	4.4	− 42.1	16.9
	1d + 2→Z1A	0.5	− 38.7	12.0
	1d + Z1A → MC2A	− 5.6	− 32.5	4.1
	1d + Z1A → TS2A	− 2.7	− 45.1	10.7
	1d + Z1A → Z2A	− 25.9	− 51.2	− 10.6
1e	**1e + 2→MC1A**	− 7.7	− 40.5	4.4
	1e + 2→TS1A	3.7	− 40.0	15.7
	1e + 2→Z1A	− 0.1	− 43.7	12.9
	1e + Z1A → MC2A	− 5.3	− 40.5	6.7
	1e + Z1A → TS2A	− 2.1	− 46.9	11.9
	1e + Z1A → Z2A	− 24.6	− 50.5	− 9.6

Scheme 5. It should be emphasized that, each time, the attachment of a further nitroethene molecule is easy from a kinetic point of view and, at the same time, beneficial from the thermodynamic point of view of the whole process because it is associated with a decrease in the Gibbs free energy of the reacting system by 9-12 kcal/mol.

Next, we verified the susceptibility of other CNAs mentioned on Scheme 1 to polymerization initiated by nitrone **2**. It was discovered that each of these processes is carried out according to a very similar mechanism as in the case of nitroethene. The first stage is always the formation of a labile, zwitterionic adduct, to which another CNA molecule may easily be added.

3.2 BET study of the polymerization reaction between nitroethene 1a and (Z)-C,N-diphenylnitrone 2

In order to characterize the bonding changes along the polymerization reaction of nitroethene (**1a**) and

(Z)-C,N-diphenylnitrone (**2**), a BET study of the key stages of this reaction was carried out. In the first stage of this reaction, we stand out six different topological phases (Table 2 and Fig. 2).

Phase I, 2.43 Å ≤ *d*(O1–N2) < 2.45 Å, 2.47 Å ≥ *d*(N2–C3) > 2.46 Å, 5.29 Å ≥ *d*(O1–C4) > 3.94 Å and 2.50 Å ≤ *d*(C4–C5) < 2.54 Å, begins at **MC1A**, which is a discontinuous point of the IRC from **TS1A** toward the intermediate **Z1A**. The ELF topological analysis of **MC1A** divulges slight changes in the ELF valence basins electron populations of substrates **1a** and **2** (see Table 2). The population of V(O1,N2), V(N2,C3) and V(C4,C5) disynaptic basins progressively increases, but population of V'(C4,C5) disynaptic basin remains unchanged.

At **P1A**, *Phase II* begins, 2.45 Å ≤ *d*(O1–N2) < 2.54 Å, 2.46 Å ≥ *d*(N2–C3) > 2.45 Å, 3.94 Å ≥ *d*(O1–C4) > 3.25 Å and 2.54 Å ≤ *d*(C4–C5) < 2.67 Å, which is described by a cusp *C* catastrophe. At this point, the first most relevant change along the reaction path takes place; the two V(C4,C5) and V'(C4,C5) disynaptic basins have merged into a V(C4,C5) disynaptic basin integrating 3.44e. This change is related to the double-bond rupture in the nitroethene **1a** molecule, with a demand energy cost of 7.4 kcal/mol (Table 2). In this phase, we can find the transition state (**TS1A**) of the reaction of **1a** and **2**: *d*(O1–N2) = 2.50 Å, *d*(N2–C3) = 2.45 Å, *d*(O1–C4) = 3.47 Å and *d*(C4–C5) = 2.61 Å.

Phase III, *d*(O1–N2) = 2.54 Å, *d*(N2–C3) = 2.45 Å, 3.25 Å ≥ *d*(O1–C4) > 3.19 Å and 2.67 Å ≤ *d*(C4–C5) < 2.68 Å, starts at **P2A**. This point is characterized by a fold $F^{\dagger}$ catastrophe. In this phase, we observed the formation of a new V(C5) monosynaptic basin integrating 0.55e and decreased the value of V(C4,C5) disynaptic basin, which in this phase integrating 2.84e.

At **P3A** begins *Phase IV*, 2.54 Å ≤ *d*(O1–N2) < 2.56 Å, *d*(N2–C3) = 2.45 Å, 3.19 Å ≥ *d*(O1–C4) > 3.08 Å and 2.68 Å ≤ *d*(C4–C5) < 2.71 Å. This point is characterized by fold $F^{\dagger}$ catastrophe, in which the V(C5) monosynaptic basin divides into two V(C5) and V'(C5) monosynaptic basins integrating 0.60e and 0.31e, respectively.

At *Phase V*, 2.56 Å ≤ *d*(O1–N2) < 2.58 Å, *d*(N2–C3) = 2.45 Å, 3.08 Å ≥ *d*(O1–C4) > 2.93 Å and 2.71 Å ≤ *d*(C4–C5) < 2.74 Å, which begins at **P4A**, the next significant topological change along the reaction path takes place. At this phase, established by a cusp *C* catastrophe the new V(O1,C4) disynaptic basin has been formed with initial population of 0.77e (Table 2). At this phase, we also observed that the population of V(O1) and V'(O1) monosynaptic basins and V(C4,C5) disynaptic basin progressively decreased, integrating 2.60e, 2.76e and 2.33e, respectively.

Finally, the last *Phase VI*, 2.58 Å ≤ *d*(O1–N2) < 2.57 Å, *d*(N2–C3) = 2.45 Å, 2.93 Å ≥ *d*(O1–C4) > 2.87 Å and 2.74 Å ≤ *d*(C4–C5) < 2.75 Å, is located between points **P5A** and **Z1A**. Here, characterized by cusp $C^{\dagger}$ catastrophe, a

Table 2 ELF valence basin populations, distances of the breaking and forming bonds and relative[a] electronic energies of the IRC points, **MC1A**–**Z1A**, defining the six phases characterizing the reaction of the nitroethene **1a** with (Z)-C,N-diphenylnitrone **2**

Structures	**1a**	**2**	**MC1A**	**P1A**	**P2A**	**P3A**	**P4A**	**P5A**	**Z1A**	**TS1A**
Catastrophes				*C*	$F^{\dagger}$	$F^{\dagger}$	*C*	$C^{\dagger}$	$C^{\dagger}$	
Phases			*I*	*II*	*III*	*IV*	*V*	*VI*	*VI*	
d(O1–N2)			2.426	2.449	2.535	2.543	2.558	2.575	2.570	2.501
d(N2–C3)			2.466	2.457	2.451	2.452	2.452	2.451	2.446	2.453
d(O1–C4)			5.293	3.938	3.245	3.188	3.078	2.933	2.867	3.474
d(C4–C5)			2.497	2.536	2.665	2.680	2.707	2.741	2.746	2.612
Δ*E*			− 1.4	7.4	7.9	6.8	6.4	5.9	5.6	8.1
V(O1,N2)		1.38	1.40	1.37	1.23	1.23	1.21	1.22	1.20	1.28
V(O1)		3.15	3.04	2.99	3.27	3.33	2.60	2.48	2.47	3.05
V'(O1)		2.94	3.02	2.97	2.83	2.83	2.76	2.62	2.57	2.92
V(N2,C3)		3.67	3.70	3.70	3.76	3.79	3.83	1.89	1.92	3.73
V'(N2,C3)								1.94	1.90	
V(C4,C5)	1.71		1.73	3.44	2.84	2.49	2.33	2.23	2.17	3.34
V'(C4,C5)	1.77		1.77							
V(C5)					0.55	0.60	0.65	0.65	0.61	
V'(C5)						0.31	0.37	0.46	0.52	
V(O1,C4)							0.77	0.97	1.11	

The stationary points **1a**, **2**, **MC1A**, **TS1A** and **Z1A** are also included. Distances are given in angstroms, Å, electron populations in average number of electrons, e, relative energies in kcal/mol^{-1}The stationary points **1a**, **2**, **MC1A**, **TS1A** and **Z1A** are also included. Distances are given in angstroms, Å, electron populations in average number of electrons, e, relative energies in kcal/mol^{-1}

[a]Relatively to the separated reagents **1a** and **2**

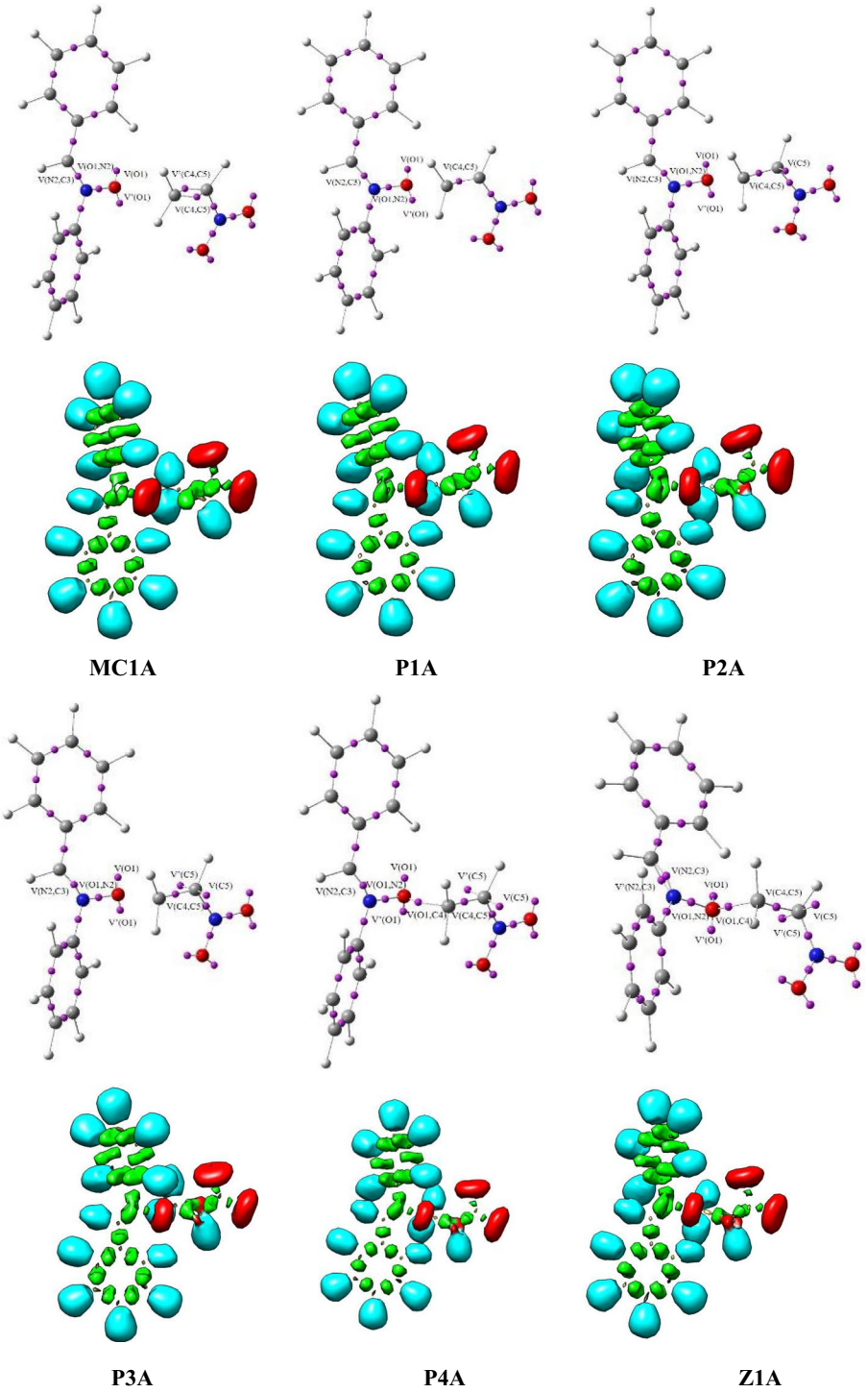

Fig. 2 ELF localization domains, represented at iso-surface values of ELF = 0.75, together with their attractor positions for the points of the IRC defining *Phases I–VI* along the reaction between nitroethene **1a** and (Z)-C,N-diphenylnitrone **2**

disynaptic basin V(N2,C3) integrating 3.83e is divided into two disynaptic basins V(N2,C3) and V'(N2,C3) integrating 1.89e and 1.94e, respectively.

In turn, addition of the second molecule of **1a** to **Z1A** can be characterized by five different topological phases (Table 3).

Phase VII, 2.75 Å $\leq d$(C4–C5) < 2.76 Å, 5.57 Å $\geq d$(C5–C6) > 4.69 Å and 2.50 Å $\leq d$(C6–C7) < 2.52 Å, starts at **MC2A**. This point is the interrupt of the IRC from **TS2A** toward the product **Z2A**. The ELF picture of **MC2A** represents small changes in ELF valence basin electron populations of **Z1A** and **1a**. ELF analysis of **MC2A** shows a slight increase in the population of V(O1,C4) and V(C6,C7) disynaptic basins. On the other hand, the population of V(C4,C5) and V'(C6,C7) disynaptic basins progressively decrease.

Table 3 ELF valence basin populations, distances of the breaking and forming bonds and relative[a] electronic energies of the IRC points, **MC2A**–**Z2A**, defining the five phases characterizing the reaction of the second molecule of nitroethene **1a** and **Z1A**

Structures	**1a**	**Z1A**	**MC2A**	**P6A**	**P7A**	**P8A**	**P9A**	**Z2A**	**TS2A**
Catastrophes				*F*	*C*	*C*	$F^{\dagger}$	$F^{\dagger}$	
Phases			*VII*	*VIII*	*IX*	*X*	*XI*	*XI*	
d(C4–C5)			2.751	2.757	2.762	2.791	2.806	2.845	2.769
d(C5–C6)			5.570	4.689	4.470	3.940	3.760	2.916	4.297
d(C6–C7)			2.500	2.522	2.541	2.633	2.678	2.811	2.564
ΔE			− 3.8	− 3.1	− 1.8	− 0.4	− 16.2	− 22.7	0.3
V(C4,C5)		2.17	2.16	2.16	2.16	2.11	2.09	2.02	2.16
V(O1,C4)		1.11	1.16	1.17	1.19	1.20	1.21	1.22	1.19
V(C6,C7)	1.71		1.78	1.78	3.49	3.34	2.53	2.02	3.47
V'(C6,C7)	1.77		1.72	1.73					
V(C5)		0.61	0.56	0.64	0.73				0.82
V'(C5)		0.52	0.51						
V(C5,C6)						1.11	1.26	1.84	
V(C7)							0.50	0.60	
V'(C7)							0.24	0.49	

The stationary points **Z1A**, **1a**, **MC2A**, **TS2A** and **Z2A** are also included. Distances are given in angstroms, Å, electron populations in average number of electrons, e, relative energies in kcal/mol^{-1}

[a]Relatively to the separated reagents **1a** and **Z1A**

At *Phase VIII*, d(C4–C5) = 2.76 Å, 4.69 Å ≥ d(C5–C6) > 4.47 Å and 2.52 Å ≤ d(C6–C7) < 2.54 Å, which begins at **P6A**, the first topological change along the reaction path takes place. In this point, described by a fold *F* catastrophe, we observed the disappearance a V'(C5) monosynaptic basin and the value of the V(C5) monosynaptic basin increased, integrating 0.64e (Table 3, Fig. 3).

Phase IX, 2.76 Å ≤ d(C4–C5) < 2.79 Å, 4.47 Å ≥ d(C5–C6) > 3.94 Å and 2.54 Å ≤ d(C6–C7) < 2.63 Å, begins at **P7A** and is featured by cusp *C* catastrophe. In this phase, the V'(C6,C7) disynaptic basin is disappearance and the value of the V(C6,C7) disynaptic basin increases, integrating 3.49e. In this phase, there is a transition state (**TS2A**) of the analyzed reaction: d(C4–C5) = 2.77 Å, d(C5–C6) = 4.30 Å and d(C6–C7) = 2.56 Å.

P8A, 2.79 Å ≤ d(C4–C5) < 2.81 Å, 3.94 Å ≥ d(C5–C6) > 3.76 Å and 2.63 Å ≤ d(C6–C7) < 2.68 Å, commences the *Phase X*, which is described by cusp *C* catastrophe. At this phase, the V(C5) monosynaptic basin disappears and a new V(C5,C6) disynaptic basin integrating 1.11e is formed. This new V(C5,C6) disynaptic basin is associated with the formation a sigma bond between C5 and C6 atoms.

At last, we distinguish the *Phase XI*, which begins at **P9A**, 2.81 Å ≤ d(C4–C5) < 2.85 Å, 3.76 Å ≥ d(C5–C6) > 2.92 Å and 2.68 Å ≤ d(C6—C7) < 2.81 Å. In this phase, located between **P9A** and **Z2A**, described by fold $F^{\dagger}$ catastrophe, we noticed that new V(C7) and V'(C7) monosynaptic basins integrating 0.50e and 0.24e are established at **P9A**. These changes are related to a high energy cost of − 16.2 kcal/mol^{-1} (Table 3).

In this section, the bonding changes arising from the BET study and their associated energy changes along the key stages of polymerization reaction between nitroethene **1a** and (Z)-C,N-diphenylnitrone **2** are summarized and described. The sequential bonding changes received from the BET analysis of the analyzed reaction are shown in Table 4, together with a simplified representation of the molecular mechanism by ELF-based Lewis-like structures. From this BET study, some appealing conclusions can be obtained: (i) the molecular mechanism of the analyzed polymerization reaction **1a** and **2** can topologically characterize eleven different phases, which have been grouped into five Groups A-E and linked to significant chemical events (Table 4); (ii) Group A, containing *Phases I* and *II*, in which the C4–C5 double bond breaks, leading to the formation of a C5 pseudoradical center. In *Phase II*, the transition state of reaction **1a** with **2** is found; (iii) Group B, containing only *Phase V*, in which the new O1–C4 single bond is formed; (iv) Group C, also contains only one *Phase VI*, which is associated with the formation of a N2–C3 double bond; (v) Phases VII–IX belong to the Group D and are associated with rupture of the C6–C7 double bond in the second molecule of **1a**; (vi) the last group, containing *Phases X–XI* in which the new C5–C6 single bond and C7 pseudoradical center are formed.

3.3 Energetical profiles and key structures for reaction involving methyl vinyl ether

CNA polymerization initiated by ether **3** is generally carried out in a rather similar way to the reaction involving nitrone **2**. The general scheme of this transformation is shown in

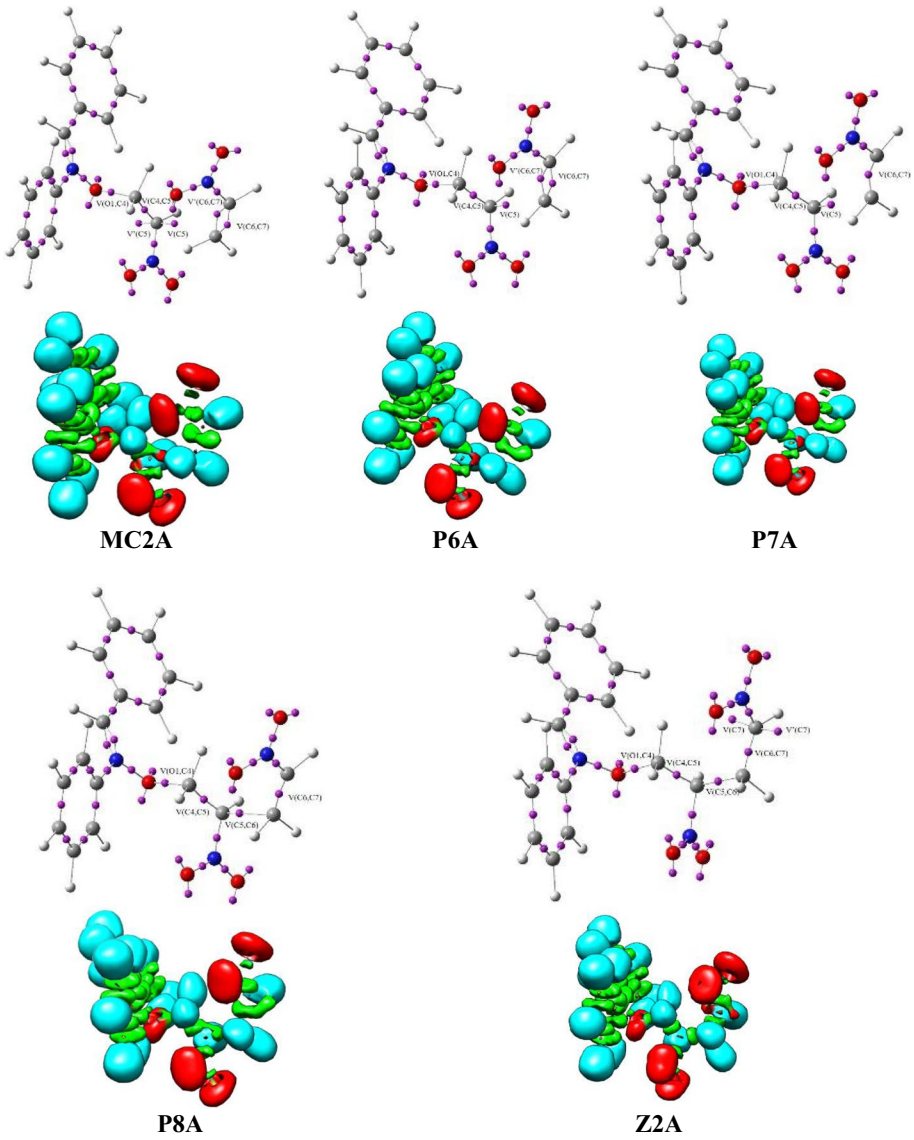

Fig. 3 ELF localization domains, represented at iso-surface values of ELF = 0.75, together with their attractor positions for the points of the IRC defining *Phases VII–XI* along the reaction between second molecule of nitroethene **1a** and intermediate **Z1A**

Scheme 6. The first stage of the process is that of formation of the molecular pre-reaction complex (**MC1B**) (Fig. 4 and Table 5). Like **MC1A**, this structure is not a CT complex, and the reaction centers within it are approaching a distance of 3.822 Å. Its conversion to zwitterion **Z1B** is carried out through transition state **TS1B**. It should be noted that the enthalpy needed to achieve **TS1B** is almost double required for **TS1A**. This is understandable, given that the global nucleophilicity of nitrone **2** is 3.64 eV, while for ether **3** it is much less, at 3.18 eV. Within **TS1B**, the distance between reaction centers is 1.948 Å. The kinetics of attaching subsequent nitroethene molecules to zwitterion **Z1B** is similar to that involved in the **1a** + **2** reaction. In particular, subsequent activation barriers for the sequence of addition of several subsequent 1a molecules do not exceed several kcal/mol. Within the analyzed TSs, reaction centers are separated from each other by a distance of approximately 2.3 Å.

Next, we verified the susceptibility of other CNAs mentioned in Scheme 1 to polymerization initiated by ether **3**. It was discovered that each of these processes is carried out via a very similar mechanism to that in the case of nitroethene. The first stage is always the formation of a labile, zwitterionic adduct, to which another CNA molecule may easily be added.

3.4 BET study of the polymerization reaction between nitroethene 1a and methyl vinyl ether 3

The BET study of the addition of the first molecule of nitroethene **1a** to methyl vinyl ether **3** indicates that this reaction is topologically characterized by five different phases. The population of the most significant valence basins of the

Table 4 Sequential bonding changes along the polymerization reaction nitroethene **1a** and (Z)-C,N-diphenylnitrone **2**, showing the equivalence between the topological characterization of the different phases and the chemical processes occurring along them. Distances are given in angstroms, Å, and relative energies are given in kcal/mol

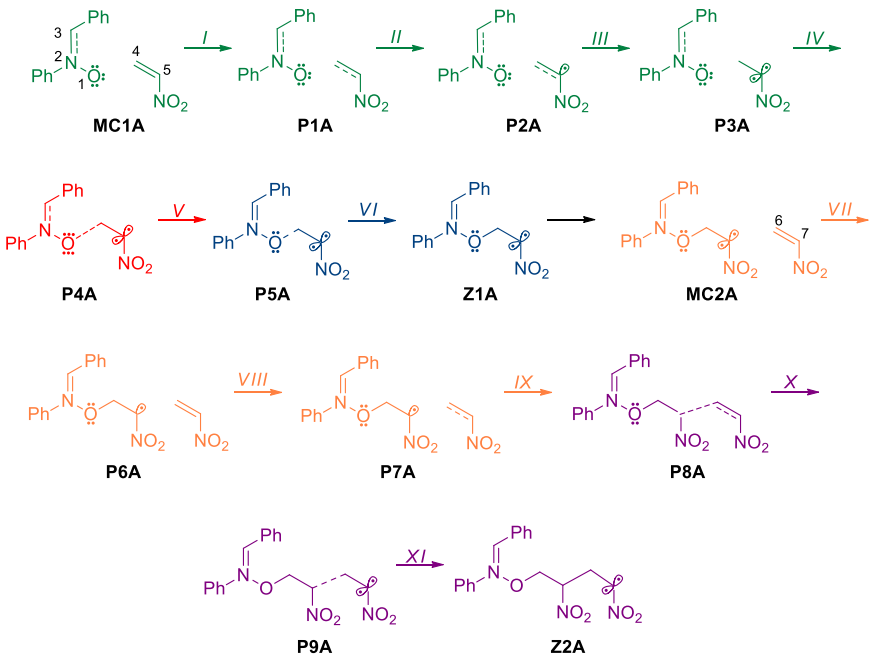

Group	Phases	d_1(O1–C4) d_2(N2–C3) d_3(C4–C5) d_4(C5–C6) d_5(C6–C7)	ΔE	Topological characterization	Chemical process
A	*I–IV*	$5.29 \geq d_1 > 3.08$ $2.47 \geq d_2 > 2.45$ $2.50 \leq d_3 < 2.71$	6.4	Merge of the V(C4,C5) and V'(C4,C5) disynaptic basins into one V(C4,C5) disynaptic basin and formation of a new V(C5) and V'(C5) monosynaptic basins	Rupture of the C4–C5 double bond
B	*V*	$3.08 \geq d_1 > 2.93$ $d_2 = 2.45$ $2.71 \leq d_3 < 2.74$	5.9	Formation of a new V(O1,C4) disynaptic basin	Formation of the O1–C4 single bond
C	*VI*	$2.93 \geq d_1 > 2.87$ $d_2 = 2.45$ $2.74 \leq d_3 < 2.75$	5.6	Split of the V(N2,C3) disynaptic basin into two V(N2,C3) and V'(N2,C3) disynaptic basins	Formation of the N2–C3 double bond
D	*VII–IX*	$2.75 \leq d_3 < 2.76$ $5.57 \geq d_4 > 4.47$ $2.50 \leq d_5 < 2.54$	−1.8	Merge of the V(C6,C7) and V'(C6,C7) disynaptic basins into one V(C6,C7) disynaptic basin	Rupture of the C6–C7 double bond
E	*X, XI*	$2.76 \leq d_3 < 2.85$ $4.47 \geq d_4 > 2.92$ $2.54 \leq d_5 < 2.81$	−22.7	Disappearance of the V(C5) monosynaptic basin and formation of V(C5,C6) disynaptic basin and two V(C7) and V′(C7) monosynaptic basins	Formation of the C5–C6 single bond

selected points of the IRC, defining the different topological phases, is included in Table 6.

Phase I, 2.51 Å $\leq d$(C1–C2) < 2.54 Å, 5.82 Å $\geq d$(C1–C3) > 4.20 Å and 2.50 Å $\leq d$(C3–C4) < 2.55 Å, begins at **MC1B**, which is the first structure of the reaction path between substrates: **1a**, **3** and **TS1B**. In this phase, only small changes in the populations of the valence basins of **MC1B** compared with **1a** and **3** are observed. The population of V'(C1,C2) and V(C3,C4) disynaptic basin progressively increases as well as the population of V(C1,C2) and V'(C3,C4) progressively decreased.

The next *Phase II*, d(C1–C2) = 2.54 Å, 4.20 Å $\geq d$(C1–C3) > 4.14 Å and 2.55 Å $\leq d$(C3–C4) < 2.56 Å, starts at **P1B**. At this point, described by the cusp *C*

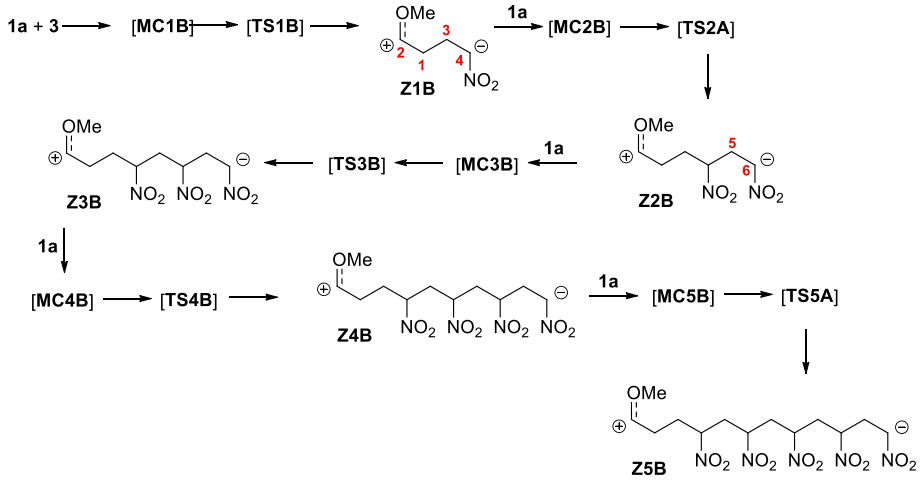

Scheme 6 Molecular mechanism of the reaction between nitroethene **1a** and methyl vinyl ether **3** according to M06-2X(PCM)/6-311 + G(d) calculations

catastrophe, the first noticeable topological change along the IRC occurs. In this phase, the two V(C3,C4) and V'(C3,C4) disynaptic basins are merged into one V(C3,C4) disynaptic basin, integrating 3.41e (Table 6 and Fig. 5). This topological change is associated with the rupture of the C3–C4 double bond in the nitroethene (**2**) molecule.

Phase III, 2.54 Å ≤ *d*(C1–C2) < 2.61 Å, 4.14 Å ≥ *d*(C1–C3) > 3.62 Å and 2.56 Å ≤ *d*(C3–C4) < 2.66 Å, begins at **P2B**. This point is characterized by a cusp *C* catastrophe. At **P2B**, the two V(C1–C2) and V'(C1,C2) disynaptic basins are integrated into one V(C1,C2) disynaptic basin, integrating 3.35e. In this phase, we observed the rupture of the C1–C2 double bond in the methyl vinyl ether (**3**) molecule. In this phase, we find the transition state (**TS1B**) of

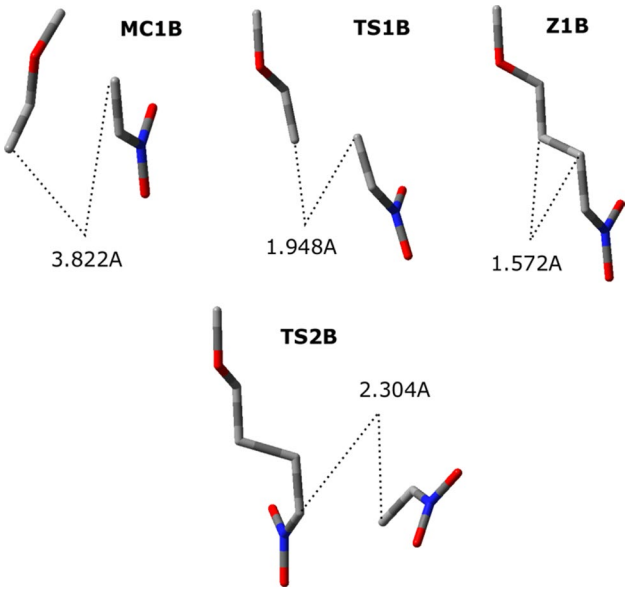

Fig. 4 Views of selected, key structures for the reaction between nitroethene **1a** and methyl vinyl ether **3** in the nitromethane solution according to M06-2X(PCM)/6-311 + G(d) calculations

studied reaction: *d*(C1–C2) = 2.60 Å, *d*(C1–C3) = 3.68 Å and *d*(C3–C4) = 2.65 Å (Table 6).

P3B starts *Phase IV*, 2.61 Å ≤ *d*(C1–C2) < 2.65 Å, 3.62 Å ≥ *d*(C1–C3) > 3.42 Å and 2.66 Å ≤ *d*(C3–C4) < 2.71 Å. In this phase, the next most relevant topological change along the reaction path is observed. At this point, a new V(C1,C3) disynaptic basin integrating 0.59e is created. In this phase, we also observed that the value of the V(C1,C2) and V(C3,C4) disynaptic basins decreased, 2.91e and 3.14, respectively. This topological change can be associated with the formation of the C1–C3 single bond, taking place at a C1–C3 distance of 3.617 Å. These changes are related to a high energy cost of 13.4 kcal/mol (Table 6).

Phase V, the last phase, 2.65 Å ≤ *d*(C1–C2) < 2.73 Å, 3.42 Å ≥ *d*(C1–C3) > 3.02 Å and 2.71 Å ≤ *d*(C3–C4) < 2.79 Å, starts at **P4B** and ends at the zwitterion product **Z1B** and is described by a fold $F^{\dagger}$ catastrophe. At this phase, the last important change along the reaction path takes place: A new V(C4) monosynaptic basin is created integrating 0.53e, which is related to the formation of a pseudoradical center on the C4 atom.

In turn, the reaction zwitterion **Z1B** with second molecule of nitroethene **1a** can be characterized by four different phases (Table 7).

Phase VI, 2.80 Å ≤ *d*(C3–C4) < 2.81 Å, 5.20 Å ≥ *d*(C4–C5) > 4.41 Å and 2.51 Å ≤ *d*(C5–C6) < 2.55 Å, begins at the **MC2B**, which is the first structure of the reaction path between **Z1B** + **1a** and **TS2B**. The ELF picture of **MC2B** represents small changes in ELF valence basin electron populations of **Z1B** and **1a**. ELF analysis of **MC2B** shows a slight increase in the population of V(C5,C6), V'(C5,C6) disynaptic basin, as well as the population of V(C3,C4) disynaptic basin progressively decreases.

At **P5B**, *Phase VII* begins, 2.81 Å ≤ *d*(C3–C4) < 2.83 Å, 4.41 Å ≥ *d*(C4–C5) > 3.89 Å and 2.55 Å ≤ *d*(C5–C6) < 2.65 Å. At this phase, established by cusp *C* catastrophe, the V'(C5,C6) disynaptic basin disappears and the valence basin

Table 5 Kinetic and thermodynamic parameters for the reaction between nitroethene **1a** and methyl vinyl ether **3** in the nitromethane solution according to M06-2X(PCM)/6-311 + G(d) calculations

Nitroalkene	Transition	ΔH (kcal/mol)	ΔS (cal/molK)	ΔG (kcal/mol)
1a	**1a + 3 → MC1A**	− 3.5	− 36.2	7.3
	1a + 3 → TS1A	14.3	− 42.2	26.9
	1a + 3 → Z1A	9.7	− 43.8	22.8
	1a + Z1a → MC2B	− 3.3	− 25.6	4.3
	1a + Z1a → TS2B	− 1.2	− 39.1	10.5
	1a + Z1a → Z2B	− 25.5	− 42.3	− 12.9
	1a + Z2B → MC3B	− 4.5	− 35.6	6.1
	1a + Z2B → TS3B	0.0	− 45.4	13.6
	1a + Z2B → Z3B	− 22.5	− 41.7	− 10.0
	1a + Z3B → MC4B	− 9.8	− 41.8	2.7
	1a + Z3B → TS4B	− 5.4	− 49.5	9.3
	1a + Z3B → Z4B	− 29.1	− 52.1	− 13.6
	1a + Z4B → MC5B	− 7.8	− 37.6	3.4
	1a + Z4B → TS5B	− 3.2	− 49.7	11.6
	1a + Z4B → Z5B	− 23.8	− 39.8	− 11.9
1b	**1b + 3 → MC1B**	− 3.9	− 37.5	7.3
	1b + 3 → TS1B	15.8	− 41.3	28.1
	1b + 3 → Z1B	12.1	− 43.2	24.9
	1b + Z1B → MC2B	− 4.1	− 32.8	5.7
	1b + Z1B → TS2B	− 1.1	− 44.5	12.2
	1b + Z1B → Z2B	− 22.7	− 47.5	− 8.6
1c	**1c + 3 → MC1B**	− 4.0	− 36.9	6.9
	1c + 3 → TS1B	14.2	− 42.5	26.9
	1c + 3 → Z1B	8.1	− 42.7	20.8
	1c + Z1B → MC2B	− 3.5	− 28.0	4.9
	1c + Z1B → TS2B	− 1.3	− 40.7	10.8
	1c + Z1B → Z2B	− 29.6	− 40.9	− 17.4
1d	**1d + 3 → MC1B**	− 4.6	− 37.6	6.6
	1d + 3 → TS1B	10.6	− 42.2	23.2
	1d + 3 → Z1B	4.2	− 42.2	16.8
	1d + Z1B → MC2B	− 4.7	− 32.5	5.0
	1d + Z1B → TS2B	− 3.5	− 46.3	10.4
	1d + Z1B → Z2B	− 25.7	− 43.1	− 12.9
1e	**1e + 3 → MC1B**	− 4.3	− 38.7	7.2
	1e + 3 → TS1B	10.4	− 43.9	23.5
	1e + 3 → Z1B	3.8	− 44.5	17.1
	1e + Z1B → MC2B	− 3.0	− 45.6	10.6
	1e + Z1B → TS2B	− 24.9	− 48.0	− 10.6

electron population of V(C5,C6) disynaptic basin increased, integrating 3.45e. This topological change can be related to the rupture of C5–C6 double bond, taking place at a C5–C6 distance of 2.548 Å. In this phase, there is a transition state (**TS2B**) of the attachment of the second nitroethene (**1a**) molecule to **Z1B**: d(C3–C4) = 2.81 Å, d(C4–C5) = 4.35 Å and d(C5–C6) = 2.56 Å (Table 7 and Fig. 6).

Phase VIII, 2.83 Å ≤ d(C3–C4) < 2.85 Å, 3.89 Å ≥ d(C4–C5) > 3.71 Å and 2.65 Å ≤ d(C5–C6) < 2.69 Å, starts at **P6B**. At this point, characterized by a fold F catastrophe, the V(C4) monosynaptic basin present at **P5B** has disappeared and a new V(C4,C5) disynaptic basin integrating 1.07e is formed. This change can be related to the

Table 6 ELF valence basin populations, distances of the breaking and forming bonds and relative[a] electronic energies of the IRC points, **MC1B**–**Z1B**, defining the five phases characterizing the reaction of the nitroethene **1a** with methyl vinyl ether **3**

Structures	**1a**	**3**	**MC1B**	**P1B**	**P2B**	**P3B**	**P4B**	**Z1B**	**TS1B**
Catastrophes				*C*	*C*	*C*	$F^{\dagger}$	$F^{\dagger}$	
Phases			*I*	*II*	*III*	*IV*	*V*	*V*	
d(C1–C2)			2.510	2.535	2.540	2.613	2.651	2.729	2.602
d(C1–C3)			5.816	4.200	4.136	3.617	3.424	3.021	3.681
d(C3–C4)			2.496	2.550	2.557	2.662	2.711	2.790	2.646
Δ*E*			− 2.9	3.9	9.1	13.4	11.2	10.3	14.9
V(C1,C2)		1.79	1.73	1.87	3.35	2.91	2.71	2.39	3.28
V'(C1,C2)		1.79	1.82	1.51					
V(C1,C3)						0.59	0.91	1.45	
V(C3,C4)	1.71		1.75	3.41	3.41	3.14	2.43	2.10	3.29
V'(C3,C4)	1.77		1.74						
V(C4)							0.53	0.54	

The stationary points **1a**, **3**, **MC1B**, **TS1B** and **Z1B** are also included. Distances are given in angstroms, Å, electron populations in average number of electrons, e, relative energies in kcal/mol^{-1}

[a]Relatively to the separated reagents **1a** and **3**

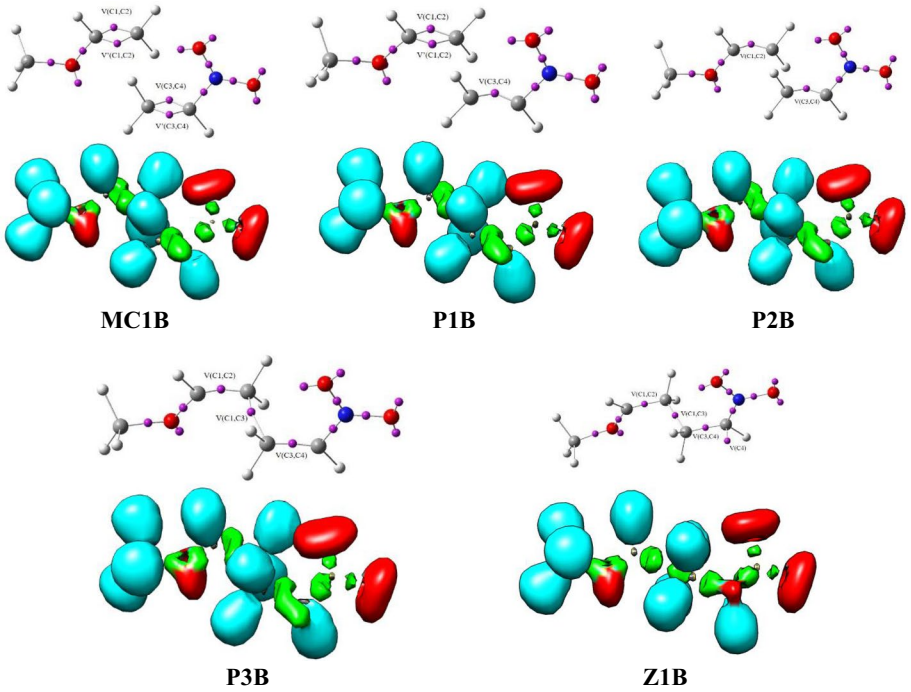

Fig. 5 ELF localization domains, represented at iso-surface values of ELF = 0.75, together with their attractor positions for the points of the IRC defining *Phases I–V* along the reaction between nitroethene **1a** and methyl vinyl ether **3**

formation of a new single bond between C4 and C5 molecules, which is taking place at a C4–C5 distance of 3.885 Å.

At last, *Phase IX*, 2.85 Å ≤ *d*(C3–C4) < 2.87 Å, 3.71 Å ≥ *d*(C4–C5) > 2.92 Å and 2.69 Å ≤ *d*(C5–C6) < 2.81 Å, begins at **P7B** and ends at the **Z2B**. At **P7**, the new V(C6) monosynaptic basin integrating 0.52e is created and the integration of V(C5,C6) disynaptic basin slightly decreased. In the **Z2B** molecule, we observed the formation of a second V'(C6) monosynaptic basin integrating 0.46e.

Table 7 ELF valence basin populations, distances of the breaking and forming bonds and relative[a] electronic energies of the IRC points, **Z1B**–**Z2B**, defining the four phases characterizing the reaction of the second molecule of nitroethene **1a** and **Z1B**

Structures	**1a**	**Z1B**	**MC2B**	**P5B**	**P6B**	**P7B**	**Z2B**	**TS2B**
Catastrophes			*C*	*C*	*F*	$F^{\dagger}$	$F^{\dagger}$	
Phases			*VI*	*VII*	*VIII*	*IX*	*IX*	
d(C3–C4)			2.800	2.805	2.831	2.845	2.865	2.807
d(C4–C5)			5.195	4.412	3.885	3.708	2.921	4.354
d(C5–C6)			2.505	2.548	2.645	2.688	2.811	2.555
Δ*E*			− 2.7	− 1.3	− 9.8	− 20.4	− 24.9	− 0.6
V(C3,C4)		2.10	2.08	2.07	2.01	2.00	1.96	2.05
V(C4)		0.54	0.57	0.64				0.67
V(C5,C6)	1.71		1.73	3.45	3.32	2.61	2.02	3.38
V'(C5,C6)	1.77		1.75					
V(C4,C5)					1.07	1.29	1.84	
V(C6)						0.52	0.51	
V'(C6)							0.46	

The stationary points **Z1B**, **1a**, **MC2B**, **TS2B** and **Z2B** are also included. Distances are given in angstroms, Å, electron populations in average number of electrons, e, relative energies in kcal·mol^{-1}

[a]Relatively to the separated reagents **1a** and **Z1B**

Based on the BET analysis of the polymerization reaction between nitroethene (**1a**) and methyl vinyl ether (**3**), some appealing conclusions can be drawn: (i) the molecular mechanism of the key stages of the polymerization reaction **1a** with **3** can be topologically characterized by nine different phases, which have been grouped into five groups A–E and linked to significant chemical events (see Table e3–e4); (ii) Group A, containing *Phase I*, is associated with the rupture of the C3–C4 double bond in nitroethene (**1a**) molecule; in Group B, we observed the breaking C1–C2 double bond in methyl vinyl ether (**3**) molecule; (iii) Group C comprises *Phases III–V*, in which we observed the formation of a C1–C3 single bond and pseudoradical center at C4 atom; (iv) Group D, containing *Phases VI* and *VII*, is associated with connecting the second molecule of nitroethene (**1a**) and rupture of the C5–C6 double bond; (v) Group E, the last group, comprises *Phases VIII* and *IX*, in which we observed the formation of a C4–C5 single bond and C6 pseudoradical center (Table 8).

4 Conclusion

The DFT computational study shed light on the kinetic aspects as well as the molecular mechanism of zwitterionic polymerization of simple conjugated nitroalkenes. These reactions can proceed under relatively mild conditions. The exploration of reaction profiles shows that the first reaction stage exhibits evidently polar nature, whereas additions of further CNA molecules to the polynitroalkyl molecular system formed should be considered as moderate polar processes. In BET analysis of the bonding changed along the analyzed key stages of the polymerization reaction between nitroethene and (Z)-C,N-diphenylnitrone, we can distinguish eleven topologically different phases. While the first step of these polymerizations is associated with the rupture of the C4–C5 double bond in nitroethene (**1a**) molecule and formation of C5 pseudoradical center, the second step is associated with the formation of O1–C4 single and N2–C3 double bonds. The next steps are associated with breaking the C6–C7 double bond in the second molecule of **1a**, formation of C5–C6 single bond and C7 pseudoradical center. In the case of the second polymerization reaction studied between nitroethene (**1a**) and methyl vinyl ether (**3**), we can highlight nine different phases. The first stage includes breaking the C3–C4 and C1–C2 double bonds, respectively, and formation of C1–C3 single bond and C4 pseudoradical center. In the next group, we notice processes related to the attachment of a second nitroethene (**1a**) molecule, in particular rupture of the C5–C6 double bond, formation of C4–C5 single bond and C6 pseudoradical center.

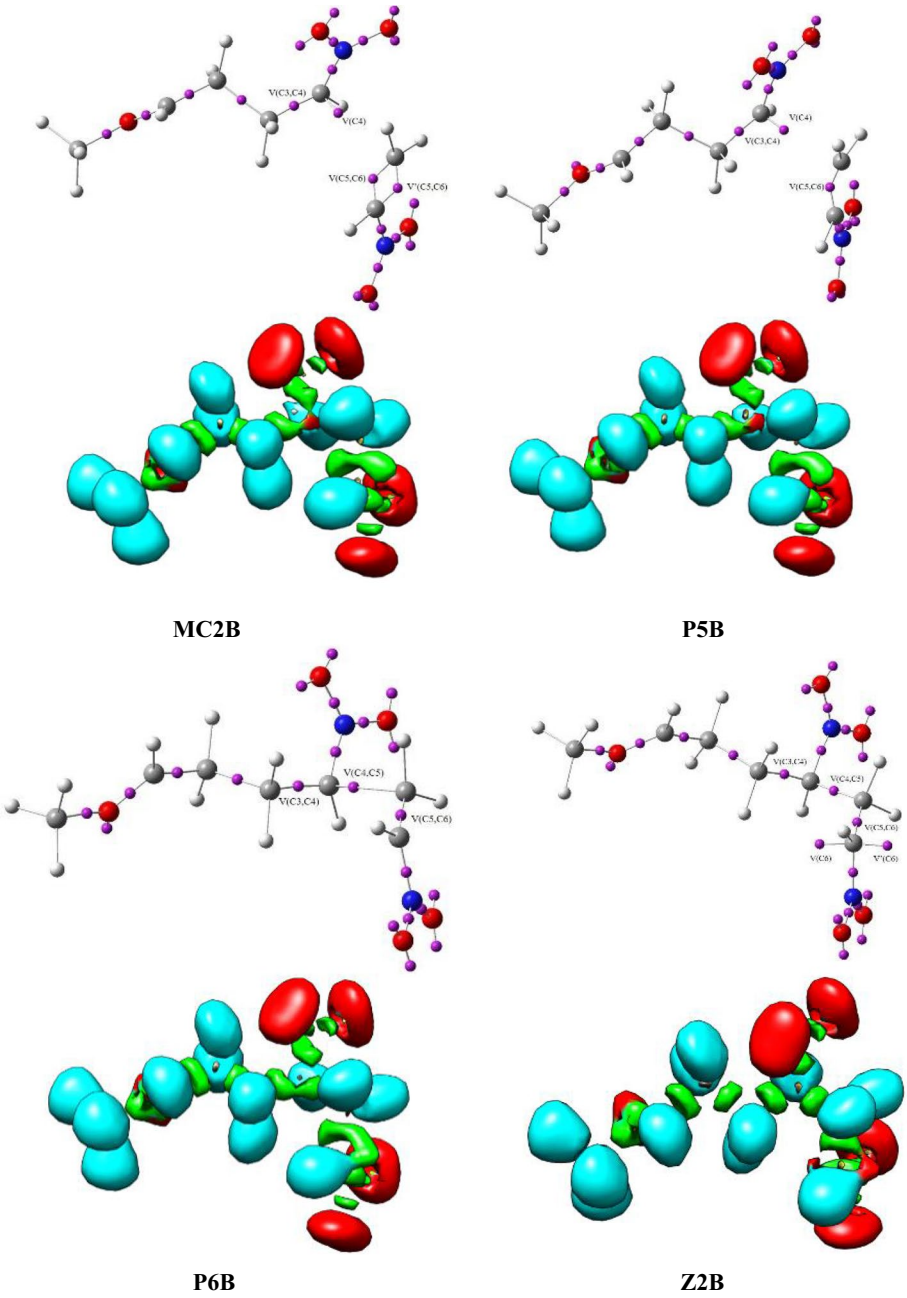

Fig. 6 ELF localization domains, represented at iso-surface values of ELF = 0.75, together with their attractor positions for the points of the IRC defining *Phases VI–IX* along the reaction between second molecule of nitroethene **1a** and intermediate **Z1B**

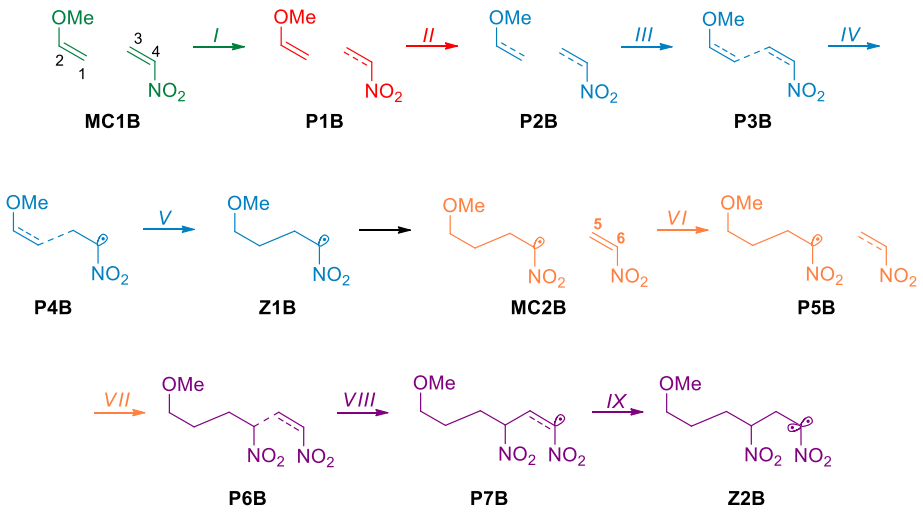

Table 8 Sequential bonding changes along the polymerization reaction nitroethene **1a** and methyl vinyl ether **3**, showing the equivalence between the topological characterization of the different phases and the chemical processes occurring along them. Distances are given in angstroms, Å, and relative energies are given in kcal/mol

Group	Phases	d_1(C1–C2) d_2(C1–C3) d_3(C3–C4) d_4(C4–C5) d_5(C5–C6)	ΔE	Topological characterization	Chemical process
A	*I*	$2.51 \leq d_1 < 2.54$ $5.82 \geq d_2 > 4.20$ $2.50 \leq d_3 < 2.55$	3.9	Merge of the V(C3,C4) and V′(C3,C4) disynaptic basins into one V(C3,C4) disynaptic basin	Rupture of the C3–C4 double bond
B	*II*	$d_1 = 2.54$ $4.20 \geq d_2 > 4.14$ $2.55 \leq d_3 < 2.56$	9.1	Merge of the V(C1,C2) and V′(C1,C2) disynaptic basins into one V(C1,C2) disynaptic basin	Rupture of the C1–C2 double bond
C	*III–V*	$2.54 \leq d_1 < 2.73$ $4.14 \geq d_2 > 3.02$ $2.56 \leq d_3 < 2.79$	10.3	Formation of a new V(C1,C3) disynaptic basin and V(C4) monosynaptic basin	Formation of the C1–C3 single bond
D	*VI, VII*	$2.80 \leq d_3 < 2.83$ $5.20 \geq d_4 > 3.89$ $2.51 \leq d_5 < 2.65$	–9.8	Merge of the V(C5,C6) and V'(C5,C6) disynaptic basins into one V(C5,C6) disynaptic basin	Rupture of the C5–C6 double bond
E	*VIII, IX*	$2.83 \leq d_3 < 2.87$ $3.89 \geq d_4 > 2.92$ $2.65 \leq d_5 < 2.81$	–24.9	Disappearance of the V(C4) monosynaptic basin and formation of V(C4,C5) disynaptic basin and V(C6) monosynaptic basin	Formation of the C4–C5 single bond

Acknowledgements This research was supported in part by PL-Grid Infrastructure in the regional computer center 'Cyfronet' in Cracow.

References

1. Agrawal JP, Hodgson RD (2007) Organic Chemistry of Explosives. Wiley & Sons, Chichester

2. Perekalin VV, Lipina ES, Berestovitskaya VM, Efremov DA (1994) Nitroalkenes: Conjugated Nitro Compounds. Wiley & Sons, Chichester
3. Sheremet EA, Tomanov RI, Trukhin EV, Berestovitskaya VM (2004) Synthesis of 4-Aryl-5-nitro-1,2,3-triazoles. Russ J Org Chem 40:594–595
4. Łapczuk-Krygier A, Ponikiewski Ł, Jasiński R (2014) The crystal structure of (1RS,4RS,5RS,6SR)-5-cyano-5-nitro-6-phenyl-bicyclo[2.2.1]hept-2-ene. Crystal Reports 59:961–963
5. Żmigrodzka M, Dresler E, Hordyjewicz-Baran Z, Kulesza R, Jasiński R (2017) A unique example of non-catalyzed [3 + 2] cycloaddition involving (2E)-3-aryl-2-nitroprop-2-enenitriles. Chem Heterocycl Compd 53:1161–1162
6. Wadel PA, Pipic A, Zeller M, Tsetsakos P (2013) Sequential Diels–Alder/[3,3]-sigmatropic rearrangement reactions of β-nitrostyrene with 3-methyl-1,3-pentadiene. Beilstein J Org Chem 9:2137–3146
7. Martıinez AR, Iglesias GYM (1998) Regio- and stereo-chemical study of the diels-alder reaction between (E)-3,4-Dimethoxy-β-nitrostyrene and 1-(Trimethylsilyloxy)buta-1,3-diene. J Chem Res (S) 4:169–169
8. Domingo LR, Ríos-Gutiérrez M, Pérez P (2016) A new model for C-C bond formation processes derived from the Molecular Electron Density Theory in the study of the mechanism of [3 + 2] cycloaddition reactions of carbenoid nitrile ylides with electron-deficient ethylenes. Tetrahedron 72:1524–1532
9. Banerji A, Gupta M, Biswas PK, Prangé T, Neuman A (2007) 1,3-Dipolar cycloadditions. Part XII—Selective cycloaddition route to 4-nitroisoxazolidine ring systems. J Heterocycl Chem 44:1045–1049
10. Sridharan V, Muthusubramanian S, Sivasubramanian S, Polborn K (2004) Diastereoselective synthesis of 2,3,4,5-tetrasubstituted isoxazolidines via 1,3-dipolar cycloaddition. Tetrahedron 60:8881–8892
11. Rembarz G, Kirchhoff B, Dongowski G (1966) Über die Reaktion von Phenylazid mit ω-Nitrostyrolen. J Prakt Chem 33:199–205
12. Jasiński R, Jasińska E, Dresler E (2017) A DFT computational study of the molecular mechanism of [3 + 2] cycloaddition reactions between nitroethene and benzonitrile N-oxides. J Mol Model 23:13–21
13. Łapczuk-Krygier A, Jaśkowska J, Jasiński R (2018) The influence of Lewis acid catalyst on the kinetic and molecular mechanism of nitrous acid extrusion from 3-phenyl-5-nitro-2-isoxazoline: DFT computational study. Chem Heterocycl Compd 52:1172–1174
14. Woliński P, Kącka-Zych A (2018) Chemistry of 2-aryl-1-cyano-1-nitroethenes. Part II. Chemical transformations. Techn Transact 2:121–137
15. Buckley GD, Scaife CW (1947) Aliphatic nitro-compounds. Part I. Preparation of nitro-olefins by dehydration of 2-nitro-alcohols. J Chem Soc 1471–1472
16. Blomquist AT, Tapp WJ, Johnson JR (1945) Polymerization of nitroölefins. The preparation of 2-Nitropropene polymer and of derived vinylamine polymers. J Am Chem Soc 67:1519–1524
17. Eremenko LT, Gafurov RG, Lisina LA (1969) Synthesis of 3-fluoro-3, 3-dinitro-1-propanol and some of its esters. Bull Acad Sci USSR div 21:695–697
18. Jasiński R, Dresler E, Mikulska M, Polewski D (2016) [3 + 2] Cycloadditions of 1-halo-1-nitroethenes with (Z)-C-(3,4,5-trimethoxyphenyl)-N-methyl-nitrone as regio- and stereocontrolled source of novel bioactive compounds: preliminary studies. Current Chem Lett 5:123–128
19. Wilkendorf R, Trénel M (1924) Zur Kenntnis aliphatischer Nitro-alkohole (II). Chem Ber 57:306–309
20. Sopova AS, Perekalin VV, Lebedeva WM, Yurchenko OI (1964) Zh Obshch Khim 34:1185–1187
21. Huisgen R, Penelle J, Mloston G, Buyle-Padias A, Hall HK Jr (1992) Can polymerization trap intermediates in 1, 3-dipolar cycloadditions? J Am Chem Soc 114:266–274
22. Jasiński R (2015) In the searching for zwitterionic intermediates on reaction paths of [3 + 2] cycloaddition reactions between 2,2,4,4-tetramethyl-3-thiocyclobutanone S-methylide and polymerizable olefins. RSC Adv 5:101045–101048
23. Jasiński R (2009) Regio- and stereoselectivity of [2 + 3]cycloaddition of nitroethene to (Z)-N-aryl-C-phenylnitrones. Collect Czech Chem Commun 74:1341–1349
24. Jasiński R (2009) The question of the regiodirection of the [2 + 3] cycloaddition reaction of triphenylnitrone to nitroethene. Chem Heterocycl Compd 45:748–749
25. Jasiński R, Mróz K, Kącka A (2016) Experimental and theoretical DFT study on synthesis of sterically crowded 2,3,3, (4)5-Tetrasubstituted-4-nitroisoxazolidines via 1,3-Dipolar cycloaddition reactions between ketonitrones and conjugated nitroalkenes. J Heterocycl Chem 53:1424–1429
26. Jasiński R (2014) Searching for zwitterionic intermediates in Hetero Diels-Alder reactions between methyl α, p-dinitrocinnamate and vinyl-alkyl ethers. Comput Theor Chem 1046:93–98
27. Jasiński R (2018) β-Trifluoromethylated nitroethenes in Diels-Alder reaction with cyclopentadiene: a DFT computational study. J Fluor Chem 206:1–7
28. Jasiński A (2016) A reexamination of the molecular mechanism of the Diels-Alder reaction between tetrafluoroethene and cyclopentadiene. React Kinet Mech Cat 119:49–57
29. Zhao Y, Truhlar DG (2008) The M06 suite of density functionals for main group thermochemistry, thermochemical kinetics, noncovalent interactions, excited states, and transition elements: two new functionals and systematic testing of four M06-class functionals and 12 other functionals. Theor Chem Account 120:215–241
30. Frisch MJ, Trucks GW, Schlegel HB, Scuseria GE, Robb MA, Cheeseman JR, Scalmani G, Barone V, Mennucci B, Petersson GA, Nakatsuji H, Caricato M, Li X, Hratchian HP, Izmaylov AF, Bloino J, Zheng G, Sonnenberg JL, Hada M, Ehara M, Toyota K, Fukuda R, Hasegawa J, Ishida M, Nakajima T, Honda Y, Kitao O, Nakai H, Vreven T, Montgomery JA, Peralta JrJE, Ogliaro F, Bearpark M, Heyd JJ, Brothers E, Kudin KN, Staroverov VN, Kobayashi R, Normand J, Raghavachari K, Rendell A, Burant JC, Iyengar SS, Tomasi J, Cossi M, Rega N, Millam JM, Klene M, Knox JE, Cross JB, Bakken B, Adamo C, Jaramillo J, Gomperts R, Stratmann RE, Yazyev O, Austin AJ, Cammi R, Pomelli C, Ochterski JW, Martin RL, Morokuma K, Zakrzewski VG, Voth GA, Salvador P, Dannenberg JJ, Dapprich S, Daniels AD, Farkas O, Foresman JB, Ortiz JV, Cioslowski J, Fox DJ (2009) Gaussian 09. Revision D.01. Gaussian. Inc. Wallingford CT
31. Scalmani G, Frisch MJ (2010) Continuous surface charge polarizable continuum models of solvation. I. General formalism. J Chem Phys 132:114110–114125
32. Silvi B, Savin A (1994) Classification of chemical bonds based on topological analysis of electron localization functions. Nature 371:683–686
33. Savin A, Silvi B, Colonna F (1996) Topological analysis of the electron localization function applied to delocalized bonds. Can J Chem 74:1088–1096
34. Becke AD, Edgecombe KE (1990) A simple measure of electron localization in atomic and molecular systems. J Chem Phys 92:5397–5404
35. Noury S, Krokidis K, Fuster F, Silvi B (1999) Computational tools for the electron localization function topological analysis. Comput Chem 23:597–604
36. Krokidis X, Noury S, Silvi B (1997) Characterization of elementary chemical processes by catastrophe theory. J Phys Chem A 101:7277–7282

37. Thom R (1976) Structural stability and morphogenesis: an outline of a general theory of models. Inc., Reading, Mass
38. Woodcock AER, Poston T (1974) A geometrical study of elementary catastrophes. Spinger-Verlag, Berlin
39. Gilmore R (1981) Catastrophe theory for scientists and engineers. Dover, New York